Acta Oceanol. Sin., 2016, Vol. 35, No. 2, P. 101–108
DOI: 10.1007/s13131-015-0678-8
http://www.hyxb.org.cn
E-mail: hyxbe@263.net

Major and trace element composition of surface sediments from the Southwest Indian Ridge: evidence for the incorporation of a hydrothermal component

LI Zhenggang[1, 2], CHU Fengyou[1, 2*], JIN Lu[1, 2], LI Xiaohu[1], DONG Yanhui[1], CHEN Ling[1, 2], ZHU Jihao[1]

[1] Key Laboratory of Submarine Geoscience, Second Institute of Oceanography, State Oceanic Administration (SOA), Hangzhou 310012, China

[2] Department of Earth Sciences, Zhejiang University, Hangzhou 310027, China

Received 5 December 2014; accepted 31 March 2015

Abstract

Hydrothermal materials in deep-sea sediments provide a robust tracer to the localized hydrothermal activity at mid-ocean ridges. Major, trace and rare earth element (REE) data for surface sediments collected from the ultraslow spreading Southwest Indian Ridge are presented to examine the existence of hydrothermal component. Biogenic carbonate oozes dominate all the sediment samples, with CaO content varying from 85.5% to 89.9% on a volatile-free basis. The leaching residue of bulk sediments by ~5% HCl is compositionally comparable to the Upper Continental Crust (UCC) in SiO_2, Al_2O_3, CaO, MgO, alkali elements (Rb, Cs) and high field strength elements (Nb, Ta, Zr, Hf, Ti). These detritus-hosted elements are inferred to be prominently derived from the Australian continent by means of eolian dust, while the contribution of local volcaniclastics is insignificant. In addition, the residual fraction shows a clear enrichment in Fe, Mn, and Ba compared with the UCC. Combining the positive Eu anomaly of residual fraction which is opposed to the UCC but the characteristic of hydrothermal fluids and associated precipitates occurred at mid-ocean ridges, the incorporation of localized hydrothermal component can be constrained. REE mixing calculations indicate that more than half REE within the residual fraction (~55%–60%) are derived from a hydrothermal component, which is inferred to be resulted from a diffuse fluid mineralization. The low-temperature diffuse flow may be widely distributed along the slow-ultraslow spreading ridges where crustal faults and fissures abound, and probably have a great mineralization potential.

Key words: deep-sea sediments, hydrothermal component, diffuse fluid, eolian dust, Southwest Indian Ridge

Citation: Li Zhenggang, Chu Fengyou, Jin Lu, Li Xiaohu, Dong Yanhui, Chen Ling, Zhu Jihao. 2016. Major and trace element composition of surface sediments from the Southwest Indian Ridge: evidence for the incorporation of a hydrothermal component. Acta Oceanologica Sinica, 35(2): 101–108, doi: 10.1007/s13131-015-0678-8

1 Introduction

Seafloor hydrothermal activity along the mid-ocean ridges is an important contributor to the ocean heat flux (Elderfield and Schultz, 1996). The incidence of hydrothermal plumes was proposed to be a linear function of the spreading rate on the basis of investigation on the intermediate-fast spreading mid-ocean ridges (e.g., Baker et al., 1996; Baker and German, 2004). This model predicts that the superfast spreading ridge like the East Pacific Rise yields the most extensive distribution of hydrothermal vents, while the ultraslow spreading ridge should bear the lowest frequency of hydrothermal venting due to a low magmatic budget (Baker and Urabe, 1996; Baker et al., 1996; Baker and German, 2004).

The Southwest Indian Ridge (SWIR) and the Gakkle Ridge in the Arctic Ocean were classified into a new end-member mid-ocean ridge type, characterized by ultraslow and oblique spreading (Dick et al., 2003). The amagmatic ridge segments at the SWIR and Gakkle Ridge formed by intermittent volcanism are linked to the extremely low magma supply (e.g., Dick et al., 2003; Cannat et al., 2008), whereby it is intuitively unfavorable for a hydrothermal circulation (Baker et al., 1996). However, the detailed hydrothermal surveys in recent years along those ridges surprisingly revealed that the frequency of the hydrothermal plume is higher than found in any previously surveyed areas of the mid-ocean ridges (Edmonds et al., 2003; Baker et al., 2004). These contrasting findings imply that hydrothermal activities along the ultraslow spreading ridges are probably widespread, despite of the limited reports hitherto on the confirmed active hydrothermal vents (Bach et al., 2002; German et al., 1998a; Tao et al., 2012).

Hydrothermal materials can be incorporated into deep-sea sediments in the form of sulfide debris or hydrothermal plume fallout (Dymond, 1981; Mills et al., 1993). Their primary geochemical signals can be preserved in the sediments since there is no early diagenetic element mobilization (Kuhn et al., 2000). Thus, deep-sea sediments provide a robust tracer to the localized hydrothermal activity (Dymond, 1981; Kuhn et al., 2000; Cave et al., 2002; Chavagnac et al., 2005; Mascarenhas-Pereira and Nath, 2010). In this study, we report major, trace and rare earth element composition of the deep-sea sediments collected from the SWIR with the aim to examine whether there exists a hydrothermal component.

Foundation item: The National Key Basic Research Program of China under contract Nos 2013CB429705 and 2013CB429701; the National Natural Science Foundation of China under contract Nos 41176045 and 41376067; the Scientific Research Fund of the Second Institute of Oceanography, the SOA of China under contract Nos JG1403 and JT1304.

*Corresponding author, E-mail: chu@sio.org.cn

2 Geological background and samples

The SWIR, separating the African and Antarctic plate, extends a length of approximately 7 700 km (Marks and Tikku, 2001). The ridge segments in the eastern section (35° to 69°E) are offset by several north-south trending transform faults and non-transform discontinuities with offset less than 15 km (Sauter et al., 2001; Cannat et al., 2008). In the central part of the eastern section, the ridges are surrounded by several oceanic islands and aseismic ridges such as Crozet hot spot and Del Cano Rise (Fig. 1). The ridge segment between the Indomed and Gallieni fracture zone is a relatively magmatic ridge (Sauter et al., 2001), and rarely exposes lower crustal gabbros and mantle peridotites (Zhou and Dick, 2013). It is characterized by an oblique (overall 15° obliquity) and asymmetrical spreading associated with a low-angle detachment fault (Zhao et al., 2013). In the vicinity of the detachment fault, the first active hydrothermal vent, Dragon Flag, was found during the Chinese DY115-19/20 cruise (Tao et al., 2012), and was inferred to be comparable in size with the Trans-Atlantic Geotraverse (TAG) hydrothermal mound (Zhu et al., 2010; Tao et al., 2012), the biggest one hereto found at the mid-ocean ridges.

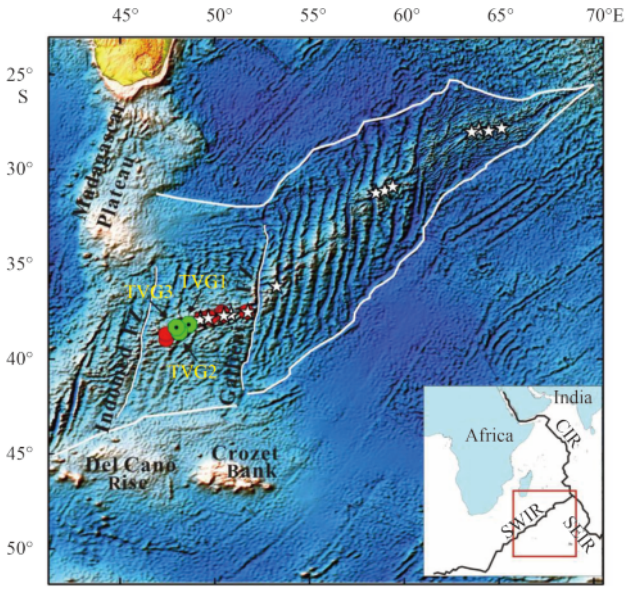

Fig. 1. Bathymetric map of the eastern portion of the SWIR, showing sample locations and major tectonic features. The TVG sites are shown as green octagon. The red dots represent the local mid-ocean ridge basalts, while the white stars represent the confirmed or inferred hydrothermal vents. The thick white lines refer to the triple junction trace. The slim white lines are used to mark the representative fracture zone where the study area is confined. FZ represents fracture zone, CIR Central Indian Ridge, SWIR Southwest Indian Ridge, and SEIR Southeast Indian Ridge.

The surface sediments used in this study were collected around 48°E by TV grab during the DY125-22 cruise in the year of 2011. The TVG sites were assigned westward downstream of the Dragon Flag hydrothermal field, and the distance between any of the two consecutive sites is no more than 50 km. The three TVG sites are all situated in the off-axis flank with shallow water depths varying from 1 662 m to 2 734 m (Table 1).

3 Analytical methods

Bulk sediment samples were divided into two parts, one of which was carried out a bulk sediment analysis. Each sample in the other part was repeatedly dissolved in dilute acid (~5% HCl) at the room temperature until no air bubble was observed in order to remove the biogenic carbonate. The leach fraction was centrifuged and separated from the residue. Leachable amorphous Fe-Mn oxides and adsorbed trace elements, together with biogenic carbonate, will be inevitably partially leached out in this procedure (Mascarenhas-Pereira and Nath, 2010). The residual fraction that is insoluble in dilute acid was expected to primarily contain the resistant siliceous detritus, and possibly the sulphide and sulphate (Chavagnac et al., 2005). Owing to the particular vulnerability to the leaching process for TVG3 sediments that consist predominantly of the biogenic carbonate and Fe-Mn crusts, the amount of their residue fraction is not large enough for a geochemical analysis. Hence, only the residual fractions of TVG1 (TVG1-1) and TVG2 (TVG2-1) sediments were carried out the geochemical analysis.

All the prepared samples were desalinated by immersing them in the ultrapure water for 30 h. The separated samples by a filter were then oven-dried at 100°C. The samples were subsequently powdered in an agate mortar to a grain size less than 74 μm. Major elements were determined using an X-ray fluorescence spectrometry, and trace elements were measured using an inductively coupled plasma spectrometer (ICP-MS) at Tianjin Institute of Geology and Mineral Resource, China Geological Survey Bureau. The analytical procedures for major and trace elements are, respectively, employed by the national standard GB/T 14506.28-2010 and GB/T 14506.30-2010. The analytical precision values are better than 5% for major elements and 10% for trace elements.

4 Results

4.1 *Major elements*

Generally, the carbonate content dominates all the bulk-sediment samples. The sediments from the TVG1 and TVG2 are pale-brown carbonate oozes, while the sediments from the TVG3 are a mixture of carbonate oozes and unconsolidated Fe-Mn crusts. The renormalized concentrations of major elements by excluding volatile content are shown in Table 1. With the exception of MnO, the bulk sediments overall show a slight variation in major element composition. The TVG1 and TVG2 sediments have very low MnO/FeOt (total iron) ratio (0.08–0.1), while TVG3 sediments have very high MnO content (4.45%) and high MnO/FeOt ratio (4.3). Regarding the residual fraction, the TVG1-1 displays similar major element composition with TVG2-1 in terms of SiO_2, Al_2O_3, MgO, K_2O, Na_2O, FeO_t and MnO, with the latter having much higher CaO content than the former (Table 1).

The anomalously high content of CaO in the TVG2-1 is probably due to the incomplete leach of organic CaO by the dilute acid (~5% HCl). This inference is based on the extremely low values of SiO_2/CaO and MgO/CaO ratios, which are incomparable to any inorganic source regardless of the Upper Continental Crust (UCC) or the oceanic crust.

4.2 *Trace elements*

The bulk-sediment samples reveal two primary characteristics: (1) each sample has much lower trace element concentration (excluding Sr) than that of its leaching residue; (2) they show a similar UCC-normalized trace element pattern (Fig. 2a). Besides, their leaching residues reveal virtually an identical UCC-

Table 1. Major and trace element compositions of the bulk sediment and residual fraction

Element	22I-SWIR-S050-TVG1	22I-SWIR-S052-TVG2	22I-SWIR-S055-TVG3	Residual fraction		UCC
				TVG1-1	TVG2-1	
South latitude/(°)	38.167	38.565	38.319			
East longitude/(°)	48.612	48.109	47.965			
Water depth/m	2 187	2 734	1 662			
SiO_2 (wt%)	3.62	5.23	3.10	62.19	59.51	66.60
TiO_2	0.07	0.08	0.07	0.88	0.78	0.64
Al_2O_3	1.72	1.83	1.37	17.34	15.66	15.40
FeOt	0.74	0.91	1.03	9.71	7.77	5.04
MgO	0.86	0.89	2.10	2.07	1.96	2.48
CaO	89.93	88.02	85.51	3.70	10.44	3.59
Na_2O	2.64	2.58	2.05	1.39	1.54	3.27
K_2O	0.21	0.28	0.19	1.93	1.71	2.80
P_2O_5	0.12	0.14	0.14	0.36	0.28	0.15
MnO	0.07	0.07	4.45	0.32	0.24	0.10
Total	99.98	100.03	100.02	99.89	99.89	100.07
LOI	43.08	42.63	41.56	16.25	20.92	
$Rb/10^{-6}$	4.57	5.73	3.46	83.00	73.40	84.00
Cs	0.25	0.31	0.21	5.34	4.50	4.90
Sr	1 500.00	1 590.00	1 880.00	218.00	396.00	320.00
Ba	208.00	322.00	78.80	2 920.00	3 630.00	628.00
Nb	0.64	0.76	0.96	12.40	10.30	12.00
Ta	0.13	0.12	0.10	0.88	0.76	0.90
Zr	5.96	8.04	6.66	146.00	116.00	193.00
Hf	0.18	0.24	0.20	4.47	3.54	5.30
U	0.18	0.20	0.50	1.69	1.41	2.70
Th	0.80	0.78	1.03	13.20	11.00	10.50
La	4.32	5.42	7.90	17.10	15.80	31.00
Ce	5.93	6.16	16.20	45.50	35.60	63.00
Pr	0.89	1.16	1.57	3.54	3.17	7.10
Nd	3.82	5.02	6.72	13.10	11.90	27.00
Sm	0.78	1.02	1.28	2.36	2.16	4.70
Eu	0.26	0.36	0.30	1.58	1.84	1.00
Gd	0.84	1.07	1.36	2.40	2.28	4.00
Tb	0.14	0.18	0.23	0.35	0.32	0.70
Dy	0.91	1.14	1.33	2.06	1.89	3.90
Ho	0.19	0.24	0.28	0.41	0.38	0.83
Er	0.56	0.70	0.78	1.27	1.13	2.30
Tm	0.09	0.10	0.11	0.20	0.18	0.30
Yb	0.54	0.64	0.67	1.30	1.18	1.96
Lu	0.08	0.10	0.10	0.20	0.18	0.31
Y	6.70	8.41	8.52	10.7	10.1	21.00
Eu/Eu*	0.98	1.05	0.69	2.01	2.52	0.69
Ce/Ce*	0.65	0.53	0.98	1.29	1.10	0.97

Notes: $Eu/Eu^*=2\times Eu_N/(Sm_N+Gd_N)$, $Ce/Ce^*=3\times Ce_N/(2\times La_N+Nd_N)$, where the subscript N represents chondrite normalization from Sun and McDonough (1989). Composition of the Upper Continental Crust (UCC) is from Rudnick and Gao (2003). $FeO_t = FeO+Fe_2O_3$.

normalized trace element pattern and a chondrite-normalized REE pattern (Figs 2a and b). However, the TVG2-1 has slightly lower trace and rare earth element contents relative to those of the TVG1-1, even though their bulk sediments reveal an opposite case (Fig. 2a). This phenomenon may be resulted from the dilution effect by the biogenic carbonate (incomplete leaching residue) which has much lower trace element content (Plank and Langmuir, 1998). This inference is supported by the excess CaO content in the TVG2-1 as noted earlier.

In a chondrite-normalized REE concentration diagram (Fig. 2b), the bulk sediments and residual fraction all show an enriched REE pattern, with the former having obviously lower REE abundance relative to the latter. Note that the sediments from both the TVG1 and TVG2 display an obviously negative Ce anomaly (Ce/Ce*=0.53–0.65) but no Eu anomaly, while TVG3 sediments display an obviously negative Eu anomaly (Eu/Eu*=0.69) but no Ce anomaly. In contrast, the residual fraction particularly shows a strong positive Eu anomaly (Eu/Eu*=2.01–2.51), and a weak positive Ce anomaly (Ce/Ce*=1.1–1.29), which is quite different to their bulk sediment composition.

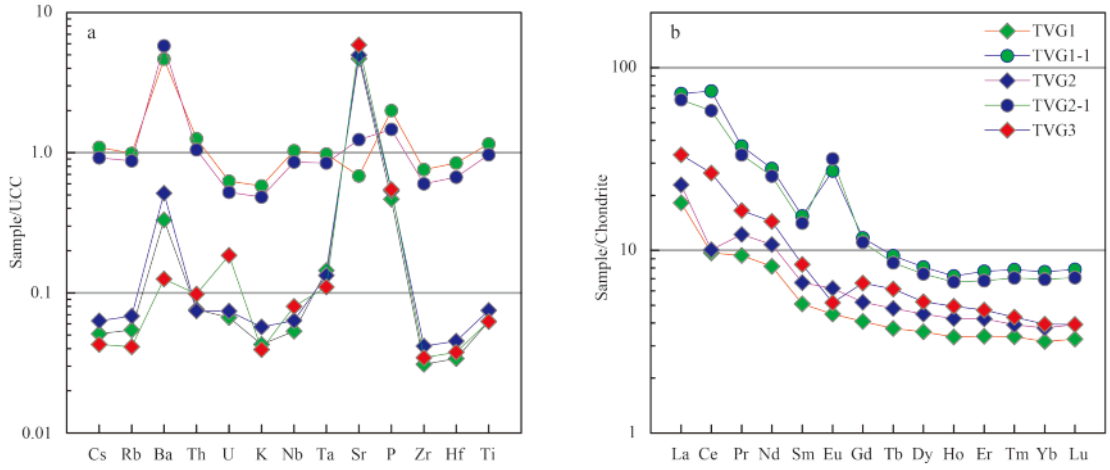

Fig. 2. The Upper Continental Crust (UCC)-normalized trace element pattern (a) and chondrite-normalized REE concentration pattern (b) of the bulk sediment and residual fraction. The trace element concentrations of the UCC are from Rudnick and Gao (2003), and the REE concentrations of the chondrite are after Sun and McDonough (1989).

5 Discussion

5.1 *Identification of the source of residual fraction*

5.1.1 *Eolian dust*

Detrital phase is the dominant component after the leaching process by about 5% HCl (Chavagnac et al., 2005; Mascarenhas-Pereira and Nath, 2010). The terrigenous detritus and local volcaniclastics are the two primary sources of SiO_2, Al_2O_3, and inorganic CaO in the pelagic sediments (Dymond, 1981). Figure 3a shows that the residual fraction nearly contains identical concentration of Si, Al, Mg and Ca (excluding TVG2-1) compared with the UCC. This may suggest that the detrital phase in the residual fraction may be primarily sourced from the continent instead of the local volcaniclastics, because mid-ocean ridge volcaniclastics often have much higher Mg but lower Si content than that of the UCC.

The other compelling evidence comes from the obvious discrepancy in their trace element composition. The outcrop in the study area is primarily of mid-ocean ridge basalts (MORB) and lacks deep-crustal rocks such as gabbros and mantle peridotites (Zhou and Dick, 2013). The local basalts have typical normal mid-ocean ridge basalt (N-MORB) characteristic that is depleted in incompatible elements (Fig. 3b). In contrast, the UCC is extremely enriched in these elements. Taking Cs as an example, its content in the UCC (Rudnick and Gao, 2003) is nearly 800 times larger than in N-MORB (Sun and McDonough, 1989). The similarity of LREE fractionation (La/Sm) between the UCC and residual fraction (Fig. 3b), thus precludes the significant involvement of the local volcaniclastics with a depleted feature.

In addition, we investigate the correlation of Al_2O_3 concentration with the trace element concentration on the basis of our five sediment samples (TVG1, TVG2, TVG3, TVG1-1 and TVG2-1) and the UCC (Rudnick and Gao, 2003). Besides, the Post-Archean Australian Shale (PAAS, Taylor and McLennan, 1995) is added to promote the confidence of the correlation coefficients. Because

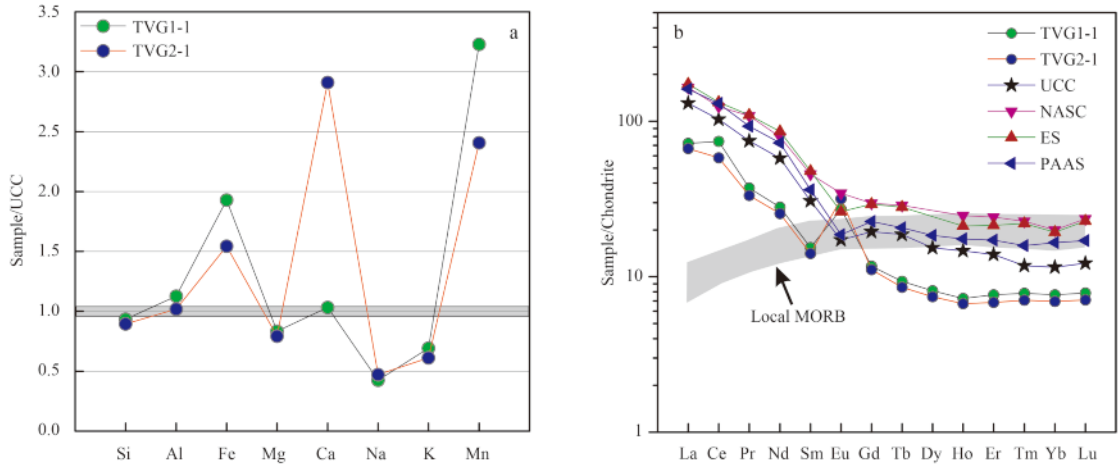

Fig. 3. Comparisons of the residual fraction with the UCC in major element composition (a), and with global terrigenous shale in REE composition (b). UCC represents Upper Continental Crust (Rudnick and Gao, 2003), NASC North American Shale Composite (Haskin et al., 1966), ES European Shale Composite (Haskin and Haskin, 1966), and PAAS Post-Archean Australian Shale (Taylor and McLennan, 1995). The local MORB field was drawn by our unpublished data.

Al_2O_3 is a representative component of the detrital phase, the higher the correlation coefficients of the target trace element with Al_2O_3 is, the larger proportion of detrital phase would be involved, and vice versa. For instance, the addition of carbonate (enriched in Sr) would extremely dilute Sr concentration in bulk pelagic sediments (Plank and Langmuir, 1998), producing a strong inverse correlation of Sr with Al_2O_3 (r<–0.9; Fig. 4). However, the alkali elements (e.g., Rb and Cs) and high filed strength elements (HFSE; e.g., Nb, Ta, Zr and Hf), together with Al_2O_3, are typically hosted by detrital phase and are barren in other components including biogenic phase, hydrothermal and hydrogenous components (Plank and Langmuir, 1998). The correlation of Al_2O_3 with the detritus-derived trace elements therefore would be independent of the dilution by a non-detritus phase. Hence, the significant correlation (r>0.9) of Al_2O_3 with the trace elements such as HFSE should be resulted from a unique source. Given that the residual fraction has comparable concentration of Rb, Cs and HFSE to the UCC (Fig. 2a), the detrital phase again is supported to be primary sourced from the continent.

It is noteworthy that the volcaniclastic deposits are very common in the deep sea (Carey and Schneider, 2011). They therefore

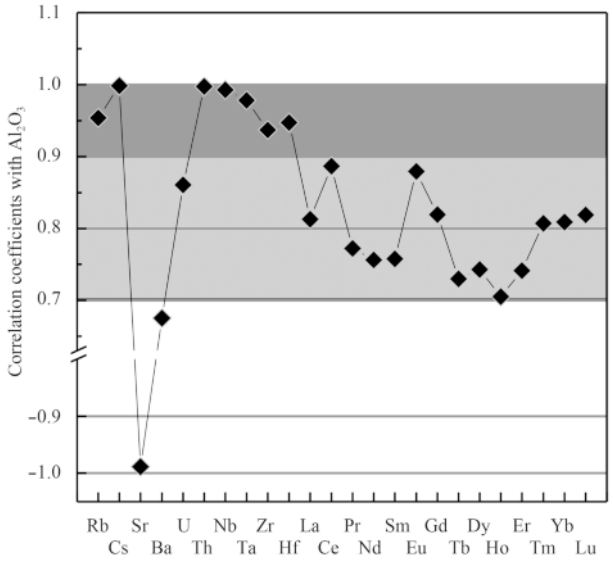

Fig. 4. Multi-element plots of correlation coefficients with Al_2O_3. The significant correlation (r>0.9) of the detritus-hosted elements including Rb, Cs, Th, Nb, Ta, Zr and Hf with Al_2O_3, suggests that these elements should have a unique source of detrital phase (see detail in the text). In contrast, the elements like Ba and REE display lower correlation coefficients (r=0.7–0.9) with Al_2O_3, indicating they have a multiple origin. Remarkably, Sr exhibits an inverse correlation with Al_2O_3, in agreement with the fact that Sr is mainly controlled by the carbonate phase.

are often considered as an end-member of the deep-sea sediment, though as a minor component (Cave et al., 2002; Chavagnac et al., 2005; Mascarenhas-Pereira and Nath, 2010). However, volcaniclastic deposits are a negligible component in our sediment samples. We interpret this particularity possibly as being due to their sedimentary location (ridge flank), where the accumulation rate of volcanic materials is relatively very low (Kuhn et al., 2000).

The mineral grains raised from continents by dust storms can be transported great distances to the ocean through the atmospheric circulation (Rea, 1994). The eolian dust input in the deep-sea sediments thus is very common and could significantly affect the sediment composition (e.g., Rea, 1994; Hovan, 1995; Chavagnac et al., 2005). In essence, the dust from different continents has a similar REE content and distribution pattern, as deduced from the global shale composition (Taylor and McLennan, 1995; Fig. 3b). Thus, it is difficult or even unlikely to constrain their provenance by their geochemical feature. Owing to the weakest atmospheric circulation in the intertropical convergence zone, the dust from the major dust sources in the Northern Hemisphere is expectedly difficult to reach the SWIR (Rea, 1994; Hovan, 1995). We therefore argue that the dust from the Australia transported by trade winds most likely accounts for the eolian flux in the SWIR sediments.

5.1.2 *Hydrothermal component*

It has been shown in Fig. 3a that the residual fraction shows an obvious enrichment in Fe and Mn relative to the UCC. The ratios of $FeOt/Al_2O_3$ (0.5–0.56) and MnO/Al_2O_3 (0.015–0.019) are much higher than those of the UCC (0.33 and 0.006, respectively), which suggests that the residual fraction contains any other components in addition to the eolian dust. This argument can be further supported by the trace element composition. If we take the detritus-derived elements (Cs, Rb and HFSE) as the compositional basement of the residual fraction (Fig. 4), any elements that below this basement line (weaker correlation with Al_2O_3) should have been superimposed by other components on the background value. For instance, the weaker correlation of REEs with Al_2O_3 (r = 0.7–0.9) could indicate a multiple origin for the REEs.

The hydrogenetic Fe-Mn crusts are enriched in Fe and Mn, but they cannot account for the Ba enrichment. The other possible contributor thus is hydrothermal component which is not only enriched in Fe and Mn but also in Ba (Dymond, 1981). This hypothesis can be readily supported by REE distribution pattern. It has been noted earlier that the continent-derived detritus bearing a negative Eu anomaly (Fig. 3b) is an important constituent in the residual fraction that inversely shows a strong positive Eu anomaly (Fig. 2b). This thus requires the involvement of a component enriched in Eu. One possibility to explain the positive Eu anomaly is the incorporation of plagioclase debris. However, the outcrop of gabbros is rare in the segment between Indomed and Gallieni fracture zone (Zhou and Dick, 2013). Besides, the incorporation of gabbros cannot explain the excess Ba, even if a positive Eu anomaly would be expected.

Alternatively, the positive Eu anomaly was resulted from the incorporation of hydrothermal component. At mid-ocean ridges, the high-temperature hydrothermal fluids are exclusively characterized by LREE enrichment and strong positive Eu anomaly (Douville et al., 1999; Allen and Seyfried Jr, 2005; Cao et al., 2012). The enhanced LREE and Eu contents in the hydrothermal fluids are independent of crustal-rock REE abundance and rock type (Allen and Seyfried Jr, 2005), but associated with the dominant ligand species which effectively transport Eu^{2+} and trivalent LREE (Bach et al., 2003; Craddock et al., 2010). However, REE fractionation during sulfide formation is notable. This is particularly evident for Eu that has much lower distribution coefficient between sulfide and fluid than other REE, which would result in weaker positive Eu anomaly in sulfides than in fluids (Mills and Elderfield, 1995; Humphris et al., 1998; Zeng et al., 1999; Rimskaya-Korsakova and Dubinin, 2003). In spite of this, hydrothermal

sulfides in most cases display a positive Eu anomaly, although a negative Eu anomaly has also been sparsely observed (Rimskaya-Korsakova and Dubinin, 2003; Tao et al., 2011).

5.2 *Estimation of the sedimentary components*

In this section, we present the assessment of the proportion of each end-member that makes up the residual fraction by using REE modeling. As noted earlier, the residual fraction consists predominantly of the eolian dust and hydrothermal component. The PAAS from western Australian (McLennan et al., 1983) was chosen to represent the dust component, because they are geographically most close to the SWIR. Figure 5a shows that they have slightly weaker LREE enrichment (La_N/Yb_N=9.73) and Eu depletion (Eu/Eu*=0.87) compared with global PAAS and the UCC (McLennan et al., 1983). It has been mentioned earlier that the composition of hydrothermal sulfides varies from vent to vent. Owing to the lack of the REE composition of in-situ hydrothermal sulfide, the OBS sulfide from the East Pacific Rise was used to represent the hydrothermal component because of its low extent of weathering (German et al., 1999). The composition of the two end-members is shown in Fig. 5a. The mass balance equation is summarized as below:

$$f_{\text{dust}} + f_{\text{sulfide}} = 1,$$

$$C^i_{\text{mix}} = f_{\text{dust}} \times C^i_{\text{dust}} + f_{\text{sulfide}} \times C^i_{\text{sulfide}},$$

where f represents the proportion of each end-member in sulfide and dust contributing to the residual fraction; and C^i is the concentration of element i. The result of calculations (Fig. 5b) shows that REE composition of the TVG1-1 and TVG2-1 can be reproduced by a mixture of 55%–60% hydrothermal sulfide and 40%–45% eolian dust. This approach therefore suggests that REE abundance of the residual fraction is dominated by hydrothermal component. The mixtures bear great resemblance to the residual faction in total REE abundance and distribution pattern, but display somewhat lower Eu anomaly relative to the residual fraction. The origin of lower positive Eu anomaly for the mixture could be resulted from the underestimation of Eu concentration for the selected end-member. The hydrothermal precipitates in the study area perhaps have greater extent of positive Eu anomaly than OBS sulfides.

5.3 *Origin of the ferromagnanese crust in TVG3 sediments*

Ferromagnanese crusts in the mid-ocean ridge could be hydrogenetic or hydrothermal origin (Kuhn et al., 1998). The hydrogenetic Fe-Mn crusts are typically characterized by positive Ce anomaly because of the oxidative scavenging of Ce from seawater (Elderfield et al., 1981), while the Fe-Mn crusts for a hydrothermal origin always display negative or no Ce anomaly (Kuhn et al., 1998). Figure 2b shows that the TVG3 sediments have no Ce anomaly, which obviously differs to the TVG1 and TVG2 sediments. The negative Ce anomaly for the TVG1 and TVG2 sediments should be an inherent feature of carbonate oozes which inherits from seawater. The lack of the negative Ce anomaly for TVG3 sediments thus requires the compensation of a component with positive Ce anomaly, which of course ought to be subject to the hydrogenetic Fe-Mn crusts.

Another evidence for the hydrogenetic Fe-Mn crusts is that the TVG3 sediments have higher U/Th and MnO/FeOt ratio than those of the TVG1 and TVG2 sediments. The high U concentration is consistent with the uptake of seawater U during oxidation process (Wen et al., 1997). Besides, MnO/FeOt ratio (4.3) of the TVG3 sediments falls in the range of hydrogenetic Fe-Mn crusts (Wen et al., 1997), but is much larger than those in the UCC and hydrothermal component (far less than 1).

5.4 *Implication for hydrothermal activity at ultraslow spreading ridge*

Hydrothermal component in deep-sea sediments could be derived from (1) near-vent sulfide debris, (2) dispersal hydrothermal plume fallout, and (3) near-vent diffuse fluids (Dymond, 1981; Mills et al., 1993). The sulfide debris transported from nearby vent by bottom current can be excluded because no sulfide interlayer has been observed in our collected sediments. Previous studies suggested that hydrothermal plume fallout can be detected over the length of tens of kilometers (German et al., 1998b). However, hydrothermal plume fallout cannot explain the excess Ba, due to the in-situ precipitation of Ba from the hydrothermal fluid once it mixes with ambient seawater (Dias et al., 2008). This inference can be further supported by the depletion

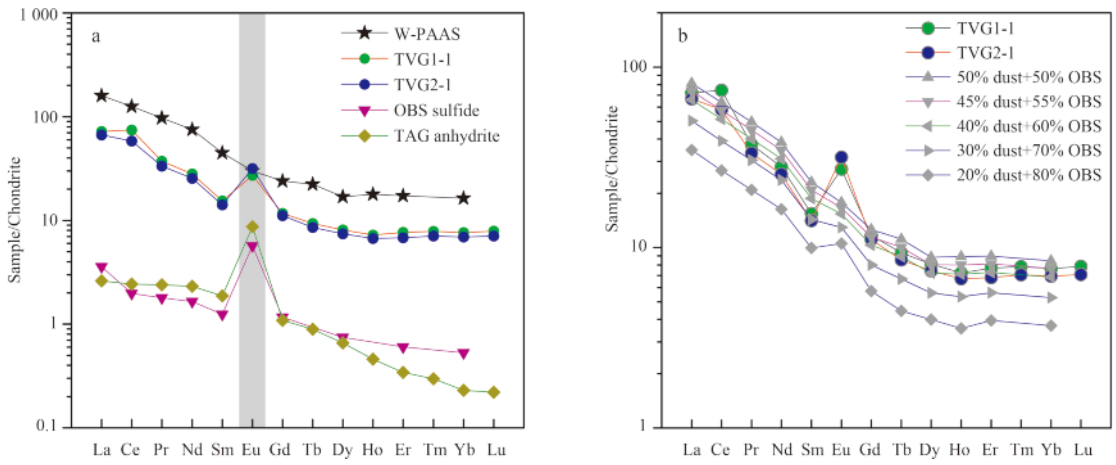

Fig. 5. The compositions of selected end-members involving REE mixing calculation (a) and the results of REE mixing calculations (b). The data of W-PAAS (the Post-Archean Australian Shale from the western Australia) are after McLennan et al. (1983). The data of OBS sulfide and TAG anhydrite are respectively from German et al. (1999) and Humphris (1998).

of Ba in plume particle (German et al., 2002). Thus, the most likely mechanism of hydrothermal component involvement in our collected sediments is the near-vent diffuse fluid mineralization.

The formation of low-temperature diffuse fluids occurred in the study area is most likely ascribed to the sub-seafloor mixing with entrained seawater, as deduced from their REE distribution pattern. In addition, mixing of seawater could increase the Eu^{3+}/Eu^{2+} ratio in the fluids due to both the increased oxygen fugacity and decreased temperature that is conducive to Eu entering into crystal lattice (Humphris et al., 1998). This possibly explains why a white smoker chimney often has stronger positive Eu anomaly than its black smoker counterpart (Mills and Elderfield, 1995), and why the diffuse fluids generated in the study area have remarkably high positive Eu anomaly.

Hydrothermal activities at the ultraslow spreading ridges are much more extensive than previous prediction (German et al., 2002; Edmonds et al., 2003; Baker et al., 2004; Tao et al., 2012). This is because the efficiency of heat supply at the ultraslow spreading ridges is heavily underestimated when neglecting the role of crustal faults and fissures, especially the detachment fault (Baker et al., 2004; Canales et al., 2007; de Martin et al., 2007; Petersen et al., 2009). High-temperature hydrothermal fluid focuses and exits through a few cracks, and discharges on the sea floor as a high-temperature black smoker. While the remaining high-temperature fluid mixes with entrained seawater and discharges on the sea floor via an irregularly distributed crack network that forms the diffuse fluid (Bemis et al., 2012). The discharge of diffuse fluid has been widely reported, such as at TAG (Schultz et al., 1996) and Lucky-Strike (Cooper et al., 2000). Actually, available data revealed that 50%–90% of the hydrothermal heat loss occurs as diffuse flow on the sea floor (Bemis et al., 2012). This suggests the diffuse hydrothermal fluids should be widely distributed at the ultraslow spreading ridges such as the SWIR. Since the low-temperature diffuse flow is more difficult than the high-temperature focused flow to be measured, their mineralization potential, especially below the sea floor, probably has been underestimated and neglected.

6 Conclusions

We carried out the major, trace and rare earth element analysis on sediment samples collected from the Southwest Indian Ridge, including three bulk sediments and two leaching residues by 5% HCl. The bulk sediments from the TVG1 and TVG2 predominantly comprise biogenic carbonate, as well as minor eolian dust and hydrothermal component, while the bulk sediments from the TVG3 primarily contain biogenic carbonate and hydrogenetic ferromagnanese crusts. Two leaching residues (TVG1-1 and TVG2-1) are mainly composed of the hydrothermal component (55%–60%) and siliceous eolian dust (40%–45%), but have insignificant contribution from the local volcaniclastics. The incorporation of hydrothermal component in the sediments is most likely via in-situ low-temperature diffuse fluid mineralization.

Acknowledgements

We are grateful to Lin Rongcheng, Cao Yezheng, and all the crew members taking part in the first Leg of the Chinese DY125-22 cruise for their efforts in sampling.

References

Allen D E, Seyfried Jr W E. 2005. REE controls in ultramafic hosted MOR hydrothermal systems: an experimental study at elevated temperature and pressure. Geochimica et Cosmochimica Acta, 69(3): 675–683

Bach W, Banerjee N R, Dick H J B, et al. 2002. Discovery of ancient and active hydrothermal systems along the ultra-slow spreading Southwest Indian Ridge 10°–16°E. Geochemistry, Geophysics, Geosystems, 3(7): 1–14

Bach W, Roberts S, Vanko D A, et al. 2003. Controls of fluid chemistry and complexation on rare-earth element contents of anhydrite from the Pacmanus subseafloor hydrothermal system, Manus Basin, Papua New Guinea. Mineralium Deposita, 38(8): 916–935

Baker E T, Chen Y J, Morgan J P. 1996. The relationship between near-axis hydrothermal cooling and the spreading rate of mid-ocean ridges. Earth and Planetary Science Letters, 142(1–2): 137–145

Baker E T, Urabe T. 1996. Extensive distribution of hydrothermal plumes along the superfast spreading East Pacific Rise, 13°30'–18°40'S. Journal of Geophysical Research, 101(B4): 8685–8695

Baker E T, Edmonds H N, Michael P J, et al. 2004. Hydrothermal venting in magma deserts: The ultraslow-spreading Gakkel and Southwest Indian Ridges. Geochemistry, Geophysics, Geosystems, 5(8): Q08002

Baker E T, German C R. 2004. On the global distribution of hydrothermal vent fields. Geophysical Monograph Series, 148: 245–266

Bemis K, Lowell R P, Farough A. 2012. Diffuse flow on and around hydrothermal vents at mid-ocean ridges. Oceanography, 25(1): 182–191

Canales J P, Sohn R A, Demartin B J. 2007. Crustal structure of the Trans-Atlantic Geotraverse (TAG) segment (Mid-Atlantic Ridge, 26°10'N): Implications for the nature of hydrothermal circulation and detachment faulting at slow spreading ridges. Geochemistry, Geophysics, Geosystems, 8(8): Q08004

Cannat M, Sauter D, Bezos A, et al. 2008. Spreading rate, spreading obliquity, and melt supply at the ultraslow spreading Southwest Indian Ridge. Geochemistry, Geophysics, Geosystems, 9(4): Q04002

Cao Zhimin, Cao Hong, Tao Chunhui, et al. 2012. Rare earth element geochemistry of hydrothermal deposits from Southwest Indian Ridge. Acta Oceanologica Sinica, 31(2): 62–69

Carey S N, Schneider J L. 2011. Chapter 7-Volcaniclastic processes and deposits in the deep-sea. Developments in Sedimentology, 63: 457–515

Cave R R, German C R, Thomson J, et al. 2002. Fluxes to sediments underlying the Rainbow hydrothermal plume at 36°14'N on the Mid-Atlantic Ridge. Geochimica et Cosmochimica Acta, 66(11): 1905–1923

Chavagnac V, German C R, Milton J A, et al. 2005. Sources of REE in sediment cores from the Rainbow vent site (36°14'N, MAR). Chemical Geology, 216(3–4): 329–352

Cooper M J, Elderfield H, Schultz A. 2000. Diffuse hydrothermal fluids from Lucky Strike hydrothermal vent field: Evidence for a shallow conductively heated system. Journal of Geophysical Research, 105(B8): 19369–19375

Craddock P R, Bach W, Seewald J S, et al. 2010. Rare earth element abundances in hydrothermal fluids from the Manus Basin, Papua New Guinea: indicators of sub-seafloor hydrothermal processes in back-arc basins. Geochimica et Cosmochimica Acta, 74(19): 5494–5513

de Martin B J, Sohn R A, Canales J P, et al. 2007. Kinematics and geometry of active detachment faulting beneath the Trans-Atlantic Geotraverse (TAG) hydrothermal field on the Mid-Atlantic Ridge. Geology, 35(8): 711–714

Dias Á S, Mills R A, Taylor R N, et al. 2008. Geochemistry of a sediment push-core from the Lucky Strike hydrothermal field, Mid-Atlantic Ridge. Chemical Geology, 247(3–4): 339–351

Dick H J B, Lin Jian, Schouten H. 2003. An ultraslow-spreading class of ocean ridge. Nature, 426(6965): 405–412

Douville E, Bienvenu P, Charlou J L, et al. 1999. Yttrium and rare earth elements in fluids from various deep-sea hydrothermal systems. Geochimica et Cosmochimica Acta, 63(5): 627–643

Dymond J. 1981. Geochemistry of Nazca plate surface sediments: An evaluation of hydrothermal, biogenic, detrital, and hydrogenous sources. Geological Society of American Memoris, 154: 133–173

Edmonds H N, Michael P J, Baker E T, et al. 2003. Discovery of abundant hydrothermal venting on the ultraslow-spreading Gakkel ridge in the Arctic Ocean. Nature, 421(6920): 252–256

Elderfield H, Hawkesworth C J, Greaves M J, et al. 1981. Rare earth element geochemistry of oceanic ferromanganese nodules and associated sediments. Geochimica et Cosmochimica Acta, 45(4): 513–528

Elderfield H, Schultz A. 1996. Mid-ocean ridge hydrothermal fluxes and the chemical composition of the ocean. Annual Review of Earth and Planetary Sciences, 24(1): 191–224

German C R, Baker E T, Mevel C, et al. 1998a. Hydrothermal activity along the southwest Indian ridge. Nature, 395(6701): 490–493

German C R, Richards K J, Rudnicki M D, et al. 1998b. Topographic control of a dispersing hydrothermal plume. Earth and Planetary Science Letters, 156(3–4): 267–273

German C R, Hergt J, Palmer M R, et al. 1999. Geochemistry of a hydrothermal sediment core from the OBS vent-field, 21°N East Pacific Rise. Chemical Geology, 155(1–2): 65–75

German C R, Colley S, Palmer M R, et al. 2002. Hydrothermal plume-particle fluxes at 13°N on the East Pacific Rise. Deep Sea Research Part I: Oceanographic Research Papers, 49(11): 1921–1940

Haskin M A, Haskin L A. 1966. Rare earths in European shales: a redetermination. Science, 154(3748): 507–509

Haskin L A, Wildeman T R, Frey F A, et al. 1966. Rare earths in sediments. Journal of Geophysical Research, 71(24): 6091–6105

Hovan S A. 1995. Late Cenozoic atmospheric circulation intensity and climatic history recorded by eolian deposition in the Eastern Equatorial Pacific Ocean, Leg 138. Proceedings of the Ocean Drilling Program, Scientific Results, 138: 615–625

Humphris S E. 1998. Rare earth element composition of anhydrite: Implications for deposition and mobility within the active TAG hydrothermal mound. Proceedings of the Ocean Drilling Program. Scientific Results, 158: 143–159

Kuhn T, Bau M, Blum N, et al. 1998. Origin of negative Ce anomalies in mixed hydrothermal–hydrogenetic Fe–Mn crusts from the Central Indian Ridge. Earth and Planetary Science Letters, 163(1–4): 207–220

Kuhn T, Burger H, Castradori D, et al. 2000. Volcanic and hydrothermal history of ridge segments near the Rodrigues Triple Junction (Central Indian Ocean) deduced from sediment geochemistry. Marine Geology, 169(3–4): 391–409

Marks K M, Tikku A A. 2001. Cretaceous reconstructions of East Antarctica, Africa and Madagascar. Earth and Planetary Science Letters, 186(3–4): 479–495

Mascarenhas-Pereira M B L, Nath B N. 2010. Selective leaching studies of sediments from a seamount flank in the Central Indian Basin: Resolving hydrothermal, volcanogenic and terrigenous sources using major, trace and rare-earth elements. Marine Chemistry, 121(1–4): 49–66

McLennan S M, Taylor S R, Eriksson K A. 1983. Geochemistry of Archean shales from the Pilbara Supergroup, western Australia. Geochimica et Cosmochimica Acta, 47(7): 1211–1222

Mills R, Elderfield H, Thomson J. 1993. A dual origin for the hydrothermal component in a metalliferous sediment core from the Mid-Atlantic Ridge. Journal of Geophysical Research, 98(B6): 9671–9681

Mills R A, Elderfield H. 1995. Rare earth element geochemistry of hydrothermal deposits from the active TAG Mound, 26°N Mid-Atlantic Ridge. Geochimica et Cosmochimica Acta, 59(17): 3511–3524

Petersen S, Kuhn K, Kuhn T, et al. 2009. The geological setting of the ultramafic-hosted Logatchev hydrothermal field (14°45'N, Mid-Atlantic Ridge) and its influence on massive sulfide formation. Lithos, 112(1–2): 40–56

Plank T, Langmuir C H. 1998. The chemical composition of subducting sediment and its consequences for the crust and mantle. Chemical Geology, 145(3–4): 325–394

Rea D K. 1994. The paleoclimatic record provided by eolian deposition in the deep sea: The geologic history of wind. Reviews of Geophysics, 32(2): 159–195

Rimskaya-Korsakova M N, Dubinin A V. 2003. Rare earth elements in sulfides of submarine hydrothermal vents of the Atlantic Ocean. Doklady Earth Sciences, 389(3): 432–436

Rudnick R L, Gao Shan. 2003. Composition of the continental crust. Treatise on Geochemistry, 3: 1–64

Sauter D, Patriat P, Rommevaux-Jestin C, et al. 2001. The Southwest Indian Ridge between 49°15'E and 57°E: Focused accretion and magma redistribution. Earth and Planetary Science Letters, 192(3): 303–317

Schultz A, Dickson P, Elderfield H. 1996. Temporal variations in diffuse hydrothermal flow at TAG. Geophysical Research Letters, 23(23): 3471–3474

Sun S S, McDonough W F. 1989. Chemical and isotopic systematics of oceanic basalts: implications for mantle composition and processes. Geological Society, London, Special Publications, 42(1): 313–345

Tao Chunhua, Li Huaiming, Huang Wei, et al. 2011. Mineralogical and geochemical features of sulfide chimneys from the 49°39'E hydrothermal field on the Southwest Indian Ridge and their geological inferences. Chinese Science Bulletin, 56(26): 2828–2838

Tao Chunhui, Lin Jian, Guo Shiqin, et al. 2012. First active hydrothermal vents on an ultraslow-spreading center: Southwest Indian Ridge. Geology, 40(1): 47–50

Taylor S R, McLennan S M. 1995. The geochemical evolution of the continental crust. Reviews of Geophysics, 33(2): 241–265

Wen X, De Carlo E H, Li Yuanhui. 1997. Interelement relationships in ferromanganese crusts from the central Pacific ocean: Their implications for crust genesis. Marine Geology, 136(3–4): 277–297

Zeng Zhigang, Zhai Hhikui, Zhao Yiyang, et al. 1999. Rare earth element geochemistry of hydrothermal sediment from the TAG hydrothermal field, mid-Atlantic ridge. Marine Geology and Quaternary Geology, 19(3): 59–66

Zhao Minghui, Qiu Xuelin, Li Jiabiao, et al. 2013. Three-dimensional seismic structure of the Dragon Flag oceanic core complex at the ultraslow spreading Southwest Indian Ridge (49°39'E). Geochemistry, Geophysics, Geosystems, 14(10): 4544–4563

Zhou Huaiyang, Dick H J B. 2013. Thin crust as evidence for depleted mantle supporting the Marion Rise. Nature, 494(11842): 195–200

Zhu Jian, Lin Jian, Chen Yongshun, et al. 2010. A reduced crustal magnetization zone near the first observed active hydrothermal vent field on the Southwest Indian Ridge. Geophysical Research Letters, 37(18): L18303